




A successful inversion of magnetic anomalies related to 2D dyke-models by a particle swarm scheme

KHALID S ESSA^{1,*} , EID R ABO-EZZ², YVES GÉRAUD³ and MARC DIRAISON³

¹Department of Geophysics, Faculty of Science, Cairo University, P.O. 12613, Giza, Egypt.

²Department of Physics, College of Science and Humanities, Prince Sattam Bin Abdulaziz University, Al-Kharj 11942, Saudi Arabia.

³GeoResources Laboratory, Université de Lorraine, Nancy 54000, France.

*Corresponding author. e-mail: khalid_sa_essa@cu.edu.eg essa@sci.cu.edu.eg

MS received 18 August 2022; revised 22 December 2022; accepted 24 December 2022

Dykes play a key role in various geologic environments. Here, we show how we employed profile magnetic data to perceive and identify the number of dykes and their parameters by a particle swarm optimiser scheme. The results deduced from this inversion include identification and estimation of the magnetic dipole moment, depth, half-width, magnetisation angle, and origin location (dyke parameters) of dykes. Two synthetic models demonstrate this scheme: the first model tests the impact of a third-order regional anomaly and the second model considers the effect of adjacent structures. Besides, we provide two case studies related to mineral exploration, *viz.*, the Parnaiba basin from Brazil and the Pishabo Lake example from Canada. The subsurface dyke parameters estimated from drilling information and the available literature were consistently matched with those achieved from our inversion scheme, thereby demonstrating the effectiveness of the particle swarm optimisation scheme.

Keywords. Particle swarm scheme; dyke; second moving; mineral exploration.

1. Introduction

The potential field data plays a significant role in expected mineral resources under the earth's surface. Specifically, the magnetic method has a wide range of applications in visualising economic sources, their spatial distribution, including the depth, involved physical and geometric properties, and recognition of related geologic structures (Sharma 1987; Abdelrahman *et al.* 2003c; Lehmann *et al.* 2015; Biswas and Acharya 2016; Adewumi and Salako 2018; Mandal *et al.* 2020; Ramesh *et al.* 2020; Balkaya and Kaftan 2021; Biswas and Rao

2021; Mehane *et al.* 2021; Essa and Diab 2022a; Essa *et al.* 2022a, b; Gokula and Sastry 2022; Mehane 2022).

Graphical and numerical interpretation methods were widely recognised to assess the subsurface dykes parameters, such as methods using characteristic curves (Koulomzine *et al.* 1970), curve-matching approaches (Gay 1963; Dondurur and Pamukcu 2003), Werner deconvolution method (Werner 1953), spectral analysis using the power band of a magnetic anomaly (Sengupta and Das 1975), Gauss–Newton method (Won 1981), damped least-squares regression (Johnson 1969),

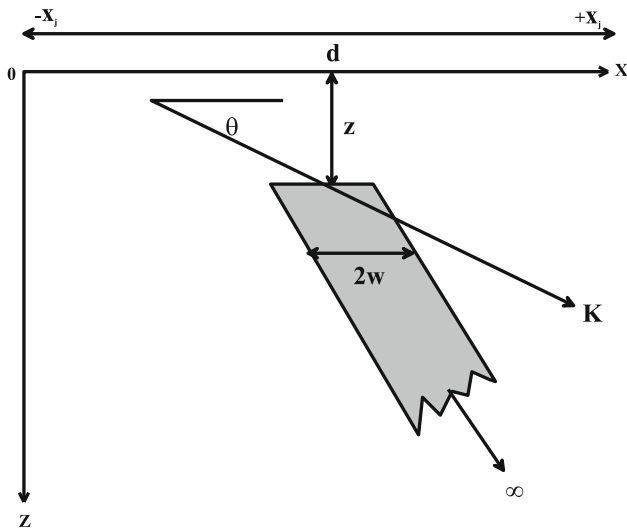


Figure 1. Schematic diagram for a 2-D inclined dyke and its parameters.

derivative-based methods (Rao *et al.* 1972; Keating and Pilkington 1990), moving-average (Abdelrahman *et al.* 2007), Fourier transform approach (Bhimasankaram *et al.* 1978), a semi-automatic method (Cooper 2012), and modular neural network method (Al-Garani 2015). However, the main drawbacks of these methods are requiring *a-priori* information on subsurface geological conditions and using few data points on the magnetic anomalies profiles to remove the regional background from the real magnetic data. Also, the sensitivity of the impeded noise in the measured field and multi-models placed at several depths affected the results.

In addition to the above-mentioned methods, Cooper (2015) presented another approach that relied on the amplitude of the analytic signal to a depth of the upper surface, dip amount, and result of susceptibility and thickness of the dyke

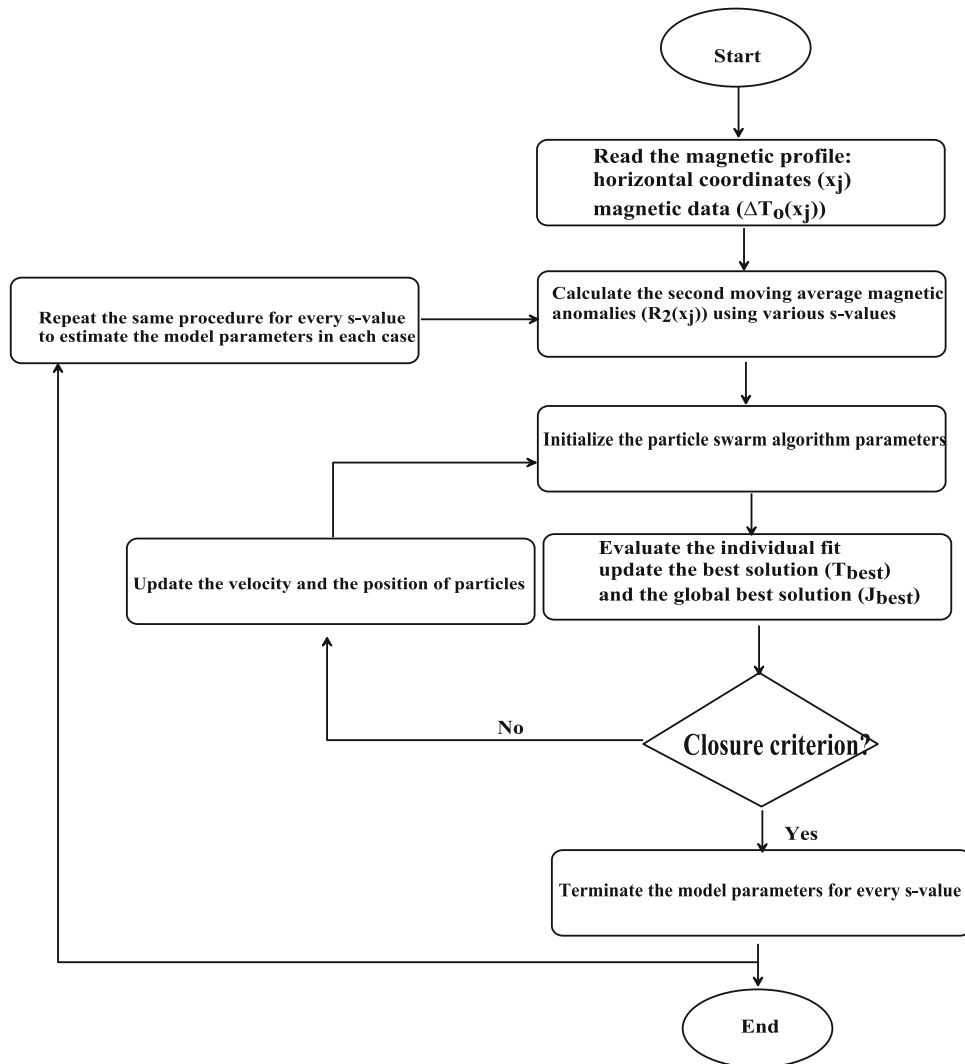


Figure 2. The flow chart of the algorithm based on particle swarm optimisation scheme.

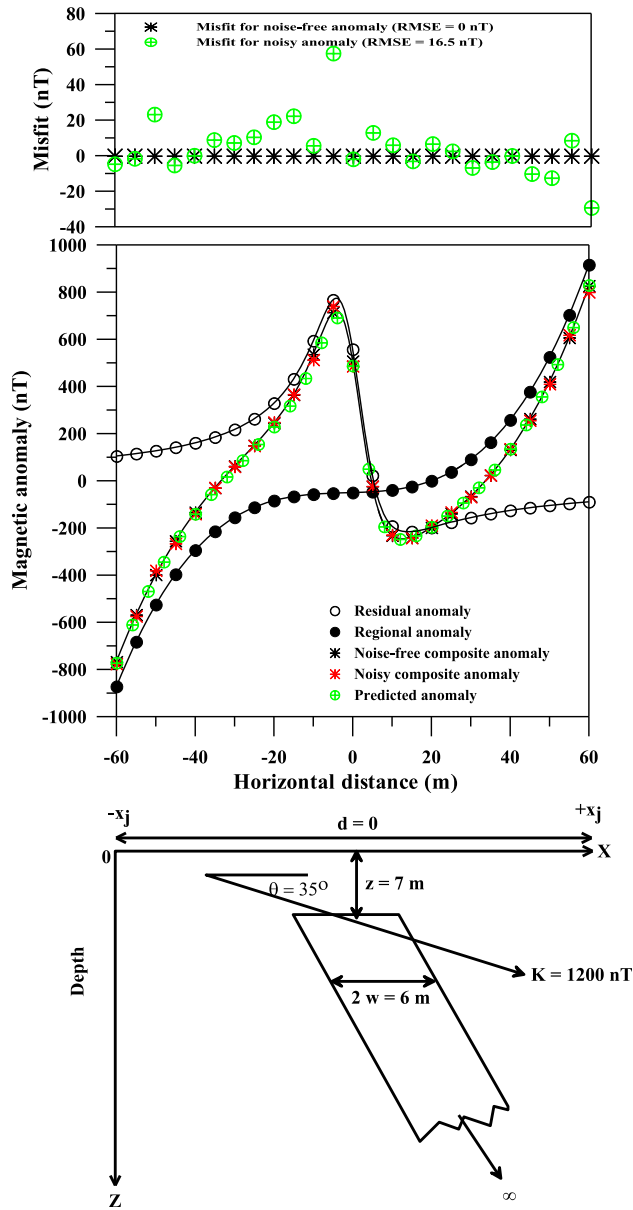


Figure 3. Inclined dyke model ($K = 1200$ nT, $\theta = 35^\circ$, $z = 7$ m, $w = 3$ m, $d = 0$, and profile length = 120 m) (white circles) and a 3rd-order regional background (black circles). Upper panel: The misfit. Middle panel: Observed (black and red asterisk) and predicted anomalies (green cross-circles). Lower panel: Geologic section.

estimation. Essa and Elhussein (2017) deliberated a new semi-automatic approach that relies on a second horizontal gradient of the observed anomaly for delimiting inclined dykes targets. Kara *et al.* (2017) established a new methodology to evaluate the dipping dyke model parameters from magnetic anomalies by applying the even component. Essa and Elhussein (2019) established an algorithm for inferring magnetic data owing to dipping dyke-like geologic structures, which utilises the horizontal gradients achieved

from the measured magnetic anomaly via filters of consecutive graticule spacings. The main difficulties within these approaches are their sensitivity to noise in data.

Here, we provide usage of the particle swarm algorithm to interpret residual magnetic anomalies measured along a profile of a 2-D inclined dyke-like geologic structure. A residual magnetic anomaly is deduced utilising the second moving average from the observed magnetic anomaly to exclude unwanted regional background up to a 3rd-order degree from the observed anomaly by applying various window lengths (s -values). The objective is to recover the characteristic inclined dyke parameters (dyke geometry parameters; figure 1), which are the magnetic dipole moment (K), depth (z), half-width (w), magnetisation angle (θ), and origin location of the dyke (d). The application of the particle swarm optimiser scheme (section 2) here was done through the utilisation of synthetic experiments (section 6), which include the presence of regional anomaly background and influence of neighbouring anomaly sources with and without random noise. In addition, it was tested on two field cases (section 7) related to mineral exploration from Brazil and Canada. Moreover, section 8 (Discussion) interprets and summarises the results attained from the present method. Finally, Conclusions (section 9) highlight and summarise the objective of the present approach.

2. The particle swarm scheme

The particle swarm scheme is considered as one of the meta-heuristic optimisation algorithms and is motivated by Kennedy and Eberhart (1995) and has various uses such as technical engineering (Yin *et al.* 2018), electromagnetics (Ciuprina *et al.* 2002), clean and solar energy (Gionfra *et al.* 2019), and engineering design problems (Acitas *et al.* 2019). Also, it is used in interpreting different geophysics data (Yang *et al.* 2015; Singh and Biswas 2016; Godio and Santilano 2018; Abdullahi *et al.* 2019; Essa 2019; Essa and Munsch 2019; Li *et al.* 2019; Essa and Elhussein 2020; Essa 2021; Qianwei *et al.* 2021; Roy *et al.* 2021; Essa and Diab 2022b; Essa *et al.* 2022a, b). The approach is explained metaphorically by considering a group of birds going on a trip for food. These birds are considered models; every model has a position and velocity. The process was initiated by giving haphazard models for the

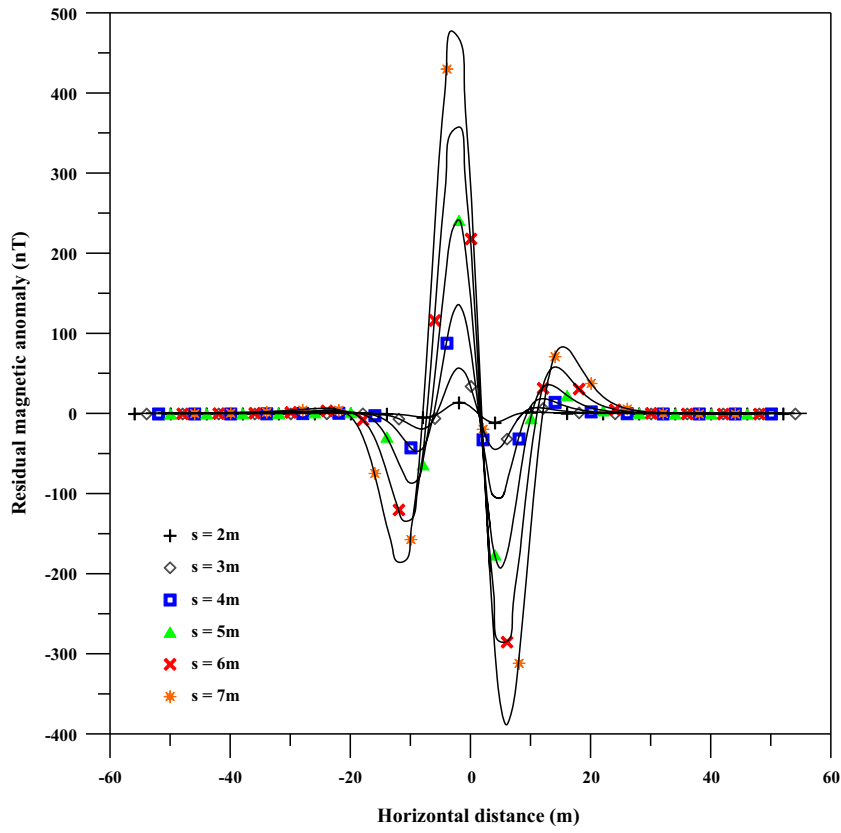


Figure 4. Residual anomaly plots for figure 3 (noise-free).

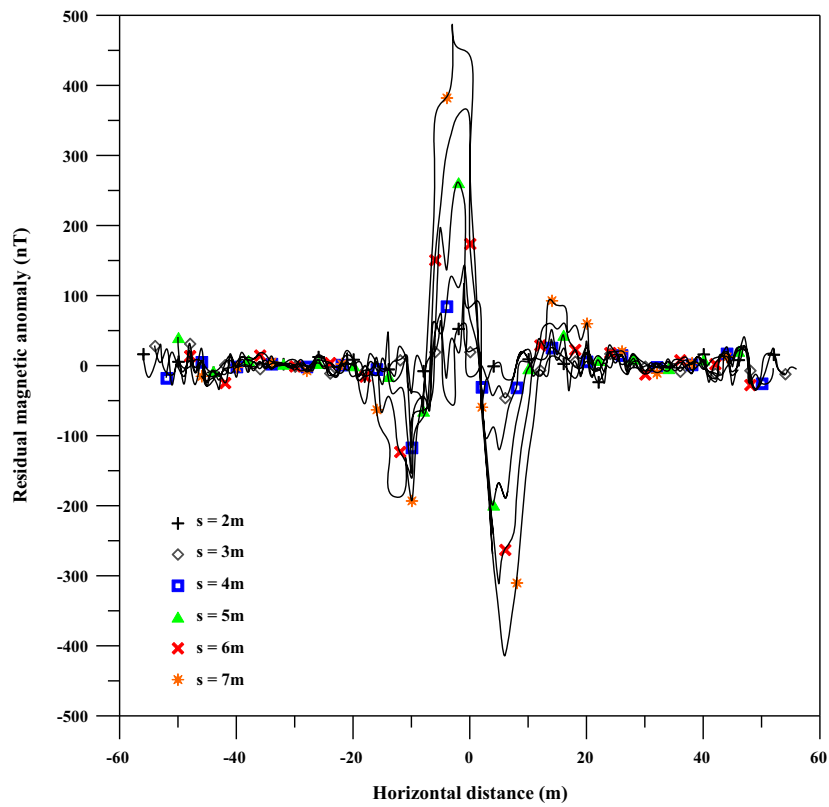


Figure 5. Residual anomaly plots for figure 3 (noisy).

Table 1. Numerical results for the synthetic example: model 1 without and with a 10% random noise.

Parameters	True values	Used ranges	Using the PSO-inversion for the second moving average anomalies							e (%)	RMSE (nT)
			$s = 2$ m	$s = 3$ m	$s = 4$ m	$s = 5$ m	$s = 6$ m	$s = 7$ m	ϕ		
Without a random noise											
K (nT)	1200	200–2000	1200	1200	1200	1200	1200	1200	1200	0	0
z (m)	7	0.1–10	7	7	7	7	7	7	7	0	0
w (m)	3	0.1–10	3	3	3	3	3	3	3	0	0
θ (°)	35	0–90	35	35	35	35	35	35	35	0	0
d (m)	0	–10–10	0	0	0	0	0	0	0	0	0
With a 10% random noise											
K (nT)	1200	200–2000	1158.4	1161.2	1172.3	1201.1	1204.7	1205.8	1183.9	1.3	16.5
z (m)	7	0.1–10	6.8	6.8	6.9	7.1	7.1	7.1	6.9	1.4	1.4
w (m)	3	0.1–10	2.8	2.9	3.0	3.0	3.1	3.1	2.9	3.9	3.9
θ (°)	35	0–90	32.5	33.8	33.0	34.2	35.3	36.4	34.1	2.5	2.5
d (m)	0	–10–10	0.1	0.1	0	0	0.1	0.1	0.1	6.6	6.6

swarm employing the limits of the various variables. The velocity and location for all models are iteratively updated by the following formulas:

$$V_j^{k+1} = c_3 V_j^k + c_1 \text{rand} \left(T_{\text{best}} - x_j^{k+1} \right) + c_2 \text{rand} \left(J_{\text{best}} - x_j^{k+1} \right), \quad (1)$$

$$x_j^{k+1} = x_j^k + V_j^{k+1}, \quad (2)$$

where x_j^k and V_j^k denote the position and velocity of the particle j , correspondingly, at iteration k ; rand denotes a randomised digit between $[0, 1]$; c_1 and c_2 are the acceleration coefficients and take a value equal to 2 (Essa *et al.* 2021); c_3 is an inertial weight that controls the model’s velocity and takes on a value of <1 ; T_{best} is the best location, which is acquired by a model, while J_{best} is the best global place reached by any model in the swarm. Afterwards, the achieved best solution (T_{best}) and the global best solution (J_{best}) are stored in memory. The model’s velocity and place are updated through an iteration procedure, which terminates when the convergence happens (Kennedy *et al.* 2001; Engelbrecht 2007). The subsequent function is used to reach the convergence:

$$\Psi_{ob} = \frac{1}{N} \sum_{j=1}^N [T_f^O(x_j) - T_f^c(x_j)]^2, \quad (3)$$

where N is the data points, T_f^O is the observed magnetic data and T_f^c is the appraised magnetic data.

3. Forward modelling

The 2-D inclined dyke magnetic anomaly (figure 1) along a profile is given by McGrath and Hood (1970) and Essa and Elhussein (2017):

$$T(x_j, z, w, \theta, d) = K \left[\sin \theta \left(\tan^{-1} \left(\frac{(x_j - d) + w}{z} \right) - \tan^{-1} \left(\frac{(x_j - d) - w}{z} \right) \right) - \frac{\cos \theta}{2} \ln \left(\frac{((x_j - d) + w)^2 + z^2}{((x_j - d) - w)^2 + z^2} \right) \right], \quad (4)$$

where x_j is the horizontal observation points, z is the depth, w is the half-width, θ is the magnetisation angle, and K is the magnetic dipole moment, which depends on the magnetic susceptibility.

4. The second moving average method

The total magnetic anomaly involves the impacts of the residual and regional anomalies, which are related to shallower and deeper geologic structures and can be expressed as:

$$T_o(x_j) = T(x_j, z, w, \theta, d) + \text{Reg}(x_j), \quad j = 1, 2, 3, \dots, N \quad (5)$$

where $T_o(x_j)$ is the measured magnetic field, $T(x_j, z, w, \theta, d)$ represents the magnetic field of the inclined dyke model (residual) and $\text{Reg}(x_j)$ is the

regional anomaly owing to deep structures. One of the furthestmost significant challenges in the processing of magnetic data is the elimination of undesirable anomalies. So, the second moving average operator usage has a benefit in this case.

Griffin (1949) is the first one to define the moving average residual magnetic anomaly. The second moving performance is one of the good techniques in unravelling the regional background anomaly proposed by a 3rd-order degree (Abdelrahman *et al.* 2003a, 2009).

Therefore, the second moving average residual magnetic anomaly is:

$$R_2(x_j, z, s) = \frac{\begin{pmatrix} 6T_o(x_j, z) \\ -4T_o(x_j + s, z) \\ -4T_o(x_j - s, z) \\ +T_o(x_j + 2s, z) \\ +T_o(x_j - 2s, z) \end{pmatrix}}{4} \quad (6)$$

where s is the graticule spacings. Moreover, the quantitative interpretation contains quite a long profile length. For short profile length, we overcome this problem by increasing the number of measurement points or increasing number of digitising intervals.

5. Estimation of dyke parameters

The dyke parameters estimation is the main objective of this study. So, the start dyke parameters (K , z , w , θ , and d) were refined and updated through the iteration progression to reach the best-fit anomaly by minimising the least-squares error (RMSE)

$$RMSE = \sqrt{\frac{1}{N} \sum_{i=1}^N [T_f^O(x_i) - T_f^c(x_i)]^2} \quad (7)$$

Finally, figure 2 reveals the flow chart for the offered scheme involves the following steps. (1) Read the magnetic data. (2) Employ the second moving average scheme with several graticule spacings to exclude the influence of the regional field. (3) Apply the particle swarm scheme to every second moving average residual anomaly to appraise the dyke parameters. (4) Compare the forward model (predicted) response, which is obtained from the calculated parameters, with the observed ones. (5) Terminate the process by a suitable closure criterion.

6. Synthetic experiment

Here, we include two models to investigate the efficacy of the algorithm.

6.1 Model 1: Presence of regional anomaly background

The 120-m long composite magnetic anomaly (T_c) (black asterisk) composed of a 2-D inclined dyke model ($K = 1200$ nT, $\theta = 35^\circ$, $z = 7$ m, $w = 3$ m,

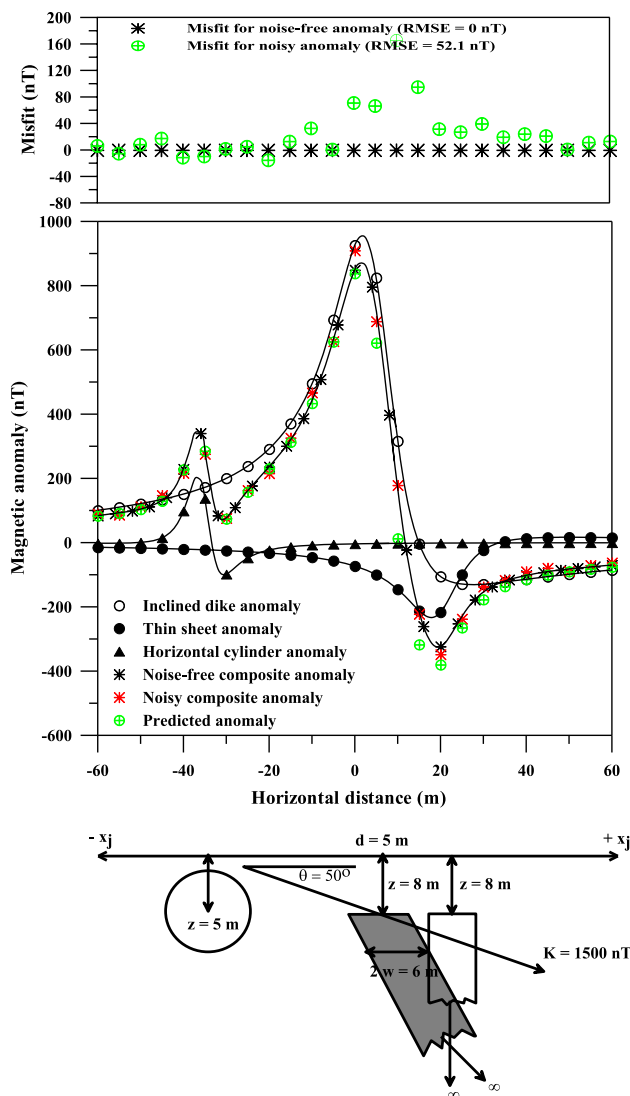


Figure 6. Inclined dyke model ($K = 1500$ nT, $z = 8$ m, $w = 3$ m, $\theta = 50^\circ$, $d = 5$ m) (white circles) affected by neighbouring structures (thin sheet is black circles and horizontal cylinder is black triangle). Upper panel: The misfit. Middle panel: Observed (black and red asterisk) and predicted anomalies (green cross-circles). Lower panel: Geologic section.

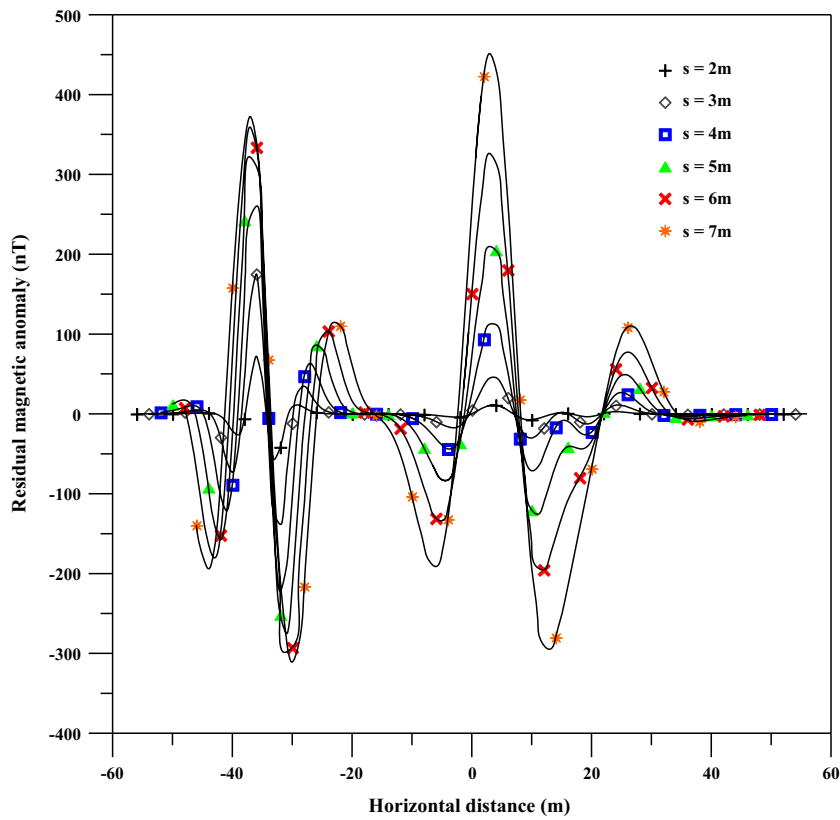


Figure 7. Residual anomaly plots for figure 6 (noise-free).

Table 2. Numerical results for the synthetic example: model 2 without and with a 10% random noise.

Parameters	True values	Used ranges	Using the PSO-inversion for the second moving average anomalies							ϕ	e (%)	RMSE (nT)
			$s = 2$ m	$s = 3$ m	$s = 4$ m	$s = 5$ m	$s = 6$ m	$s = 7$ m				
Without a random noise												
K (nT)	1500	200–2000	1500	1500	1500	1500	1500	1500	1500	1500	0	0
z (m)	8	0.1–10	8	8	8	8	8	8	8	8	0	0
w (m)	3	0.1–10	3	3	3	3	3	3	3	3	0	0
θ (°)	50	0–90	50	50	50	50	50	50	50	50	0	0
d (m)	5	–10–10	5	5	5	5	5	5	5	5	0	0
With a 10% random noise												
K (nT)	1500	200–2000	1387.2	1402.5	1429.1	1428.9	1451.7	1471.4	1428.5	4.8	52.1	
z (m)	8	0.1–10	7.3	7.2	7.5	7.4	7.2	7.5	7.4	8.1		
w (m)	3	0.1–10	2.8	2.8	2.9	3.1	2.9	2.9	2.9	3.3		
θ (°)	50	0–90	43.3	42.8	46.5	44.8	47.5	48.0	45.5	9.0		
d (m)	5	–10–10	4.3	4.6	4.4	4.7	4.8	4.6	4.6	4.6		

and $d = 0$) (residual; white circles) response combined with a third order regional anomaly (black circles) is shown in figure 3.

The procedure (figure 4) of the interpretation steps involved the separation of residual anomaly by employing the second moving average operator

for numerous s -values ($s = 2, 3, 4, 5, 6$, and 7 m) and the particle swarm process was utilised to find the dyke parameters (table 1). The optimum parameters were obtained after 200 iterations. Also, all parameter ranges are included in table 1 for K (200–2000 nT), z (1–10 m), w (1–10 m), θ

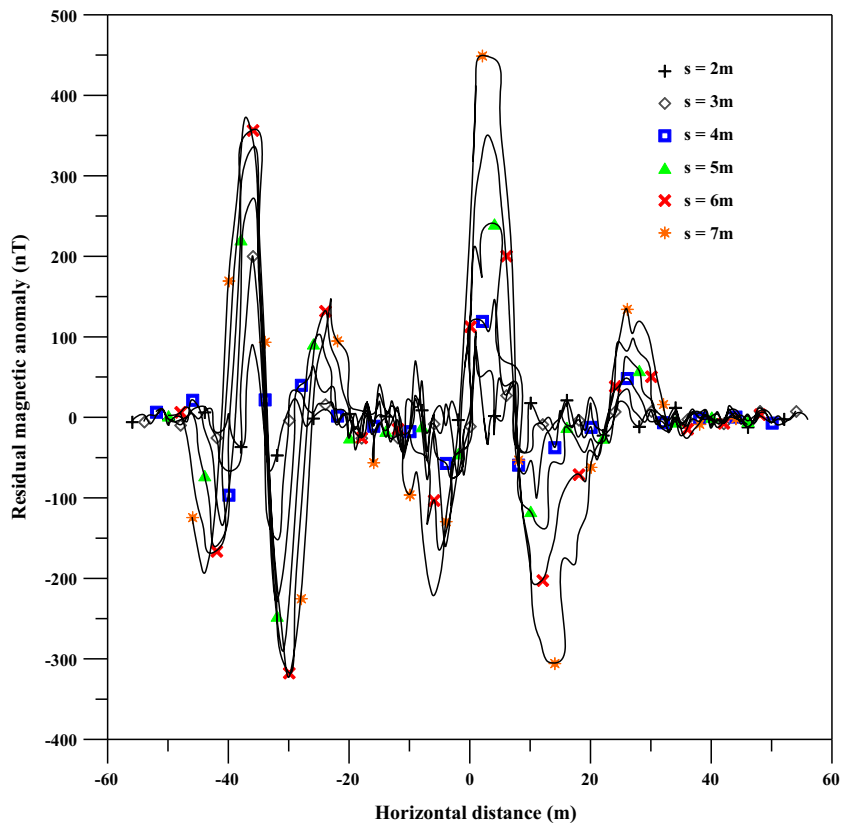


Figure 8. Residual anomaly plots for figure 6 (noisy).

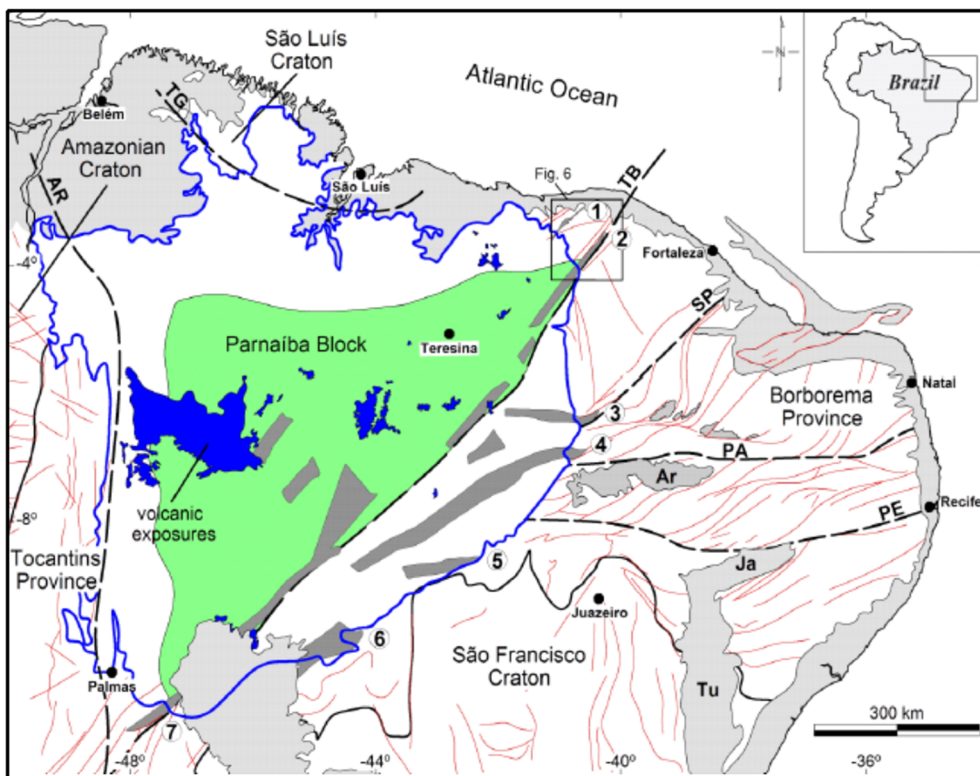


Figure 9. Geological map of the Parnaíba basin (blue line) and its Precambrian basement structures (red lines) (after de Castro et al. 2016).

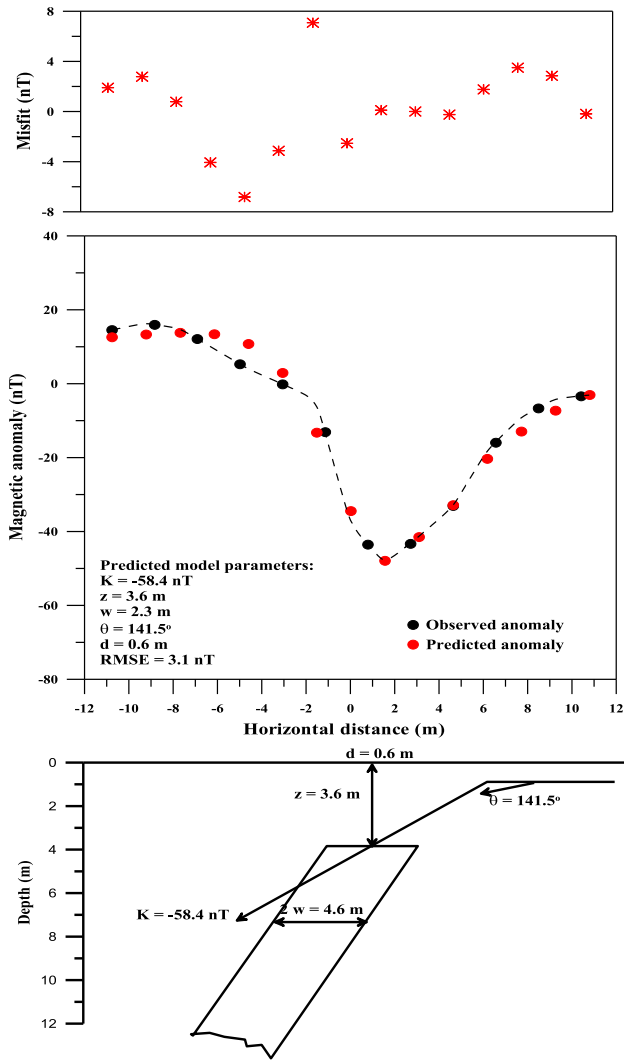


Figure 10. Upper panel: The misfit. Middle panel: Observed (black circles) and predicted anomalies (red circles) for the Parnaiba basin field example, Brazil. Lower panel: Geologic section.

(0–90°), and d (–10 to 10 m). Furthermore, the anticipated outcomes for every parameter are explained.

To check the performance reliability of the current approach, we added a 10% noise into the magnetic data of the above-mentioned model (red asterisk) (figure 3). Furthermore, figure 5 illustrates the residual anomalies for s -value equals 2, 3, 4, 5, 6, and 7 m. The predicted dyke parameters by employing the particle swarm scheme for the presumed noisy data are presented in table 1, which demonstrates the average value (ϕ) for K , z , w , θ , and d as 1183.9 nT, 6.9 m, 2.9 m, 34.1°, and 0.1 m, the e-values are 1.3%, 1.4%, 3.9%, 2.5%, and 6.6%, respectively, and the RMSE equals 16.5 nT.

The obtained results demonstrate that the suggested method can produce accurate dyke parameters and is capable of minimising the influence of regional background and noise.

6.2 Model 2: Influence of neighbouring sources

A composite magnetic profile (black asterisk) of 120 m in length due to the inclined dyke ($K = 1500 \text{ nT}$, $z = 8 \text{ m}$, $w = 3 \text{ m}$, $\theta = 50^\circ$, $d = 5 \text{ m}$) (white circles), a vertical sheet ($K = 2000 \text{ nT}$, $z = 8 \text{ m}$, $\theta = 30^\circ$, $d = 20 \text{ m}$) (black circles), and a horizontal cylinder ($K = 6000 \text{ nT}$, $z = 5 \text{ m}$, $\theta = 55^\circ$, $d = -35 \text{ m}$) (black triangles) was produced and shown in figure 6.

Estimation outlined procedure was implemented. First, the second moving average approach was employed for the combined anomaly utilising several s -values ($s = 2, 3, 4, 5, 6$, and 7 m) (figure 7). Second, the particle swarm is exploited to assess the dyke parameters (table 2). Table 2 explains that the e-values and the RMSE value are zero.

To further assess the accuracy of the established scheme, a 10% random was impeded in the combined magnetic field (red asterisk) to scrutinise the attainability of the present approach. Figure 8 illustrates the second moving average residual magnetic anomalies for the equivalent s -values. The particle swarm scheme was exploited to calculate the subsurface dyke parameters (table 2). Table 2 presents the ϕ value for K , z , w , θ , and d , which are 1428.5 nT, 7.4 m, 2.9 m, 44.8°, and 4.6 m, the amount of e-value in each parameter is 4.8%, 8.1%, 3.3%, 9%, and 4.6%, respectively, and RMSE equals 52.1 nT.

7. Case studies

To investigate the rationality and the stability of the offered scheme, two published real data sets of mineral exploration case studies from Brazil and Canada. The particle swarm optimisation scheme was implemented to these data to accomplish the optimal fit for the buried dyke parameters (K , z , w , θ , and d) and matched these results with existing geologic information and any additional geophysical outcomes.

7.1 Parnaiba basin field example, Brazil

The Parnaiba basin (figure 9) in the northeast of Brazil is considered a Phanerozoic sedimentary

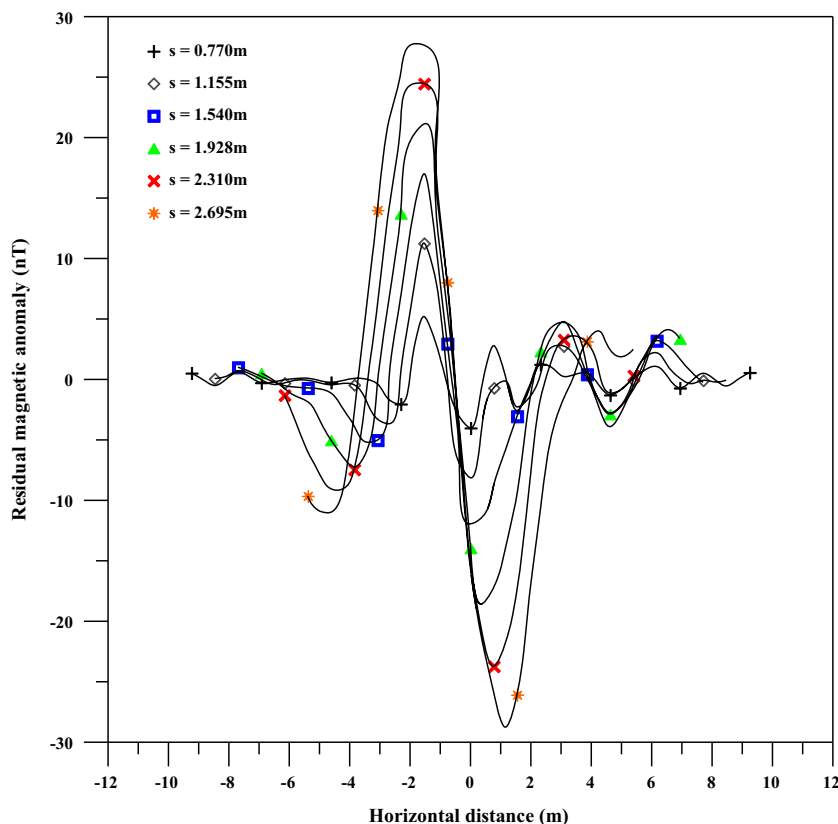


Figure 11. Residual anomaly plots for figure 10.

Table 3. Numerical results for the interpretation of magnetic anomaly of the Parnaiba basin field example, Brazil.

Using the PSO-inversion for the second moving average anomalies									
Parameters	Used ranges	$s = 0.770\text{ m}$	$s = 1.155\text{ m}$	$s = 1.540\text{ m}$	$s = 1.925\text{ m}$	$s = 2.310\text{ m}$	$s = 2.695\text{ m}$	ϕ	RMSE (nT)
K (nT)	-500–500	-57.8	-58.9	-58.2	-57.9	-58.3	-59.5	-58.4	3.1
z (m)	1–10	3.5	3.5	3.6	3.6	3.5	3.6	3.6	
w (m)	1–10	2.2	2.3	2.4	2.3	2.2	2.3	2.3	
θ (°)	0–180	140.9	141.7	143.0	140.8	141.1	141.3	141.5	
d (m)	-10–10	0.5	0.6	0.7	0.6	0.5	0.6	0.6	

Table 4. Numerical results achieved compared with other results from different approaches for the Parnaiba basin field example, Brazil.

Parameters	Silva (1989)	Asfahani and Tlas (2007)	Tlas and Asfahani (2011)	Tlas and Asfahani (2015)	Present method
K (nT)	–	-59.80	-59.82	–	-58.4 ± 0.65
z (m)	3.50	2.30	2.13	3.40	3.6 ± 0.05
w (m)	–	–	–	–	2.3 ± 0.08
θ (°)	–	47.10	41.85	41.30	141.4 ± 0.82
d (m)	–	–	0.21	–	0.6 ± 0.07

basin in South America. This basin is situated amongst the Amazonian and São Francisco cratons, inspired by moderate dense lithosphere of the

request of 160–180 km. The Precambrian crust accumulated and balanced out amid the Neoproterozoic Brasiliano orogeny (McKenzie and

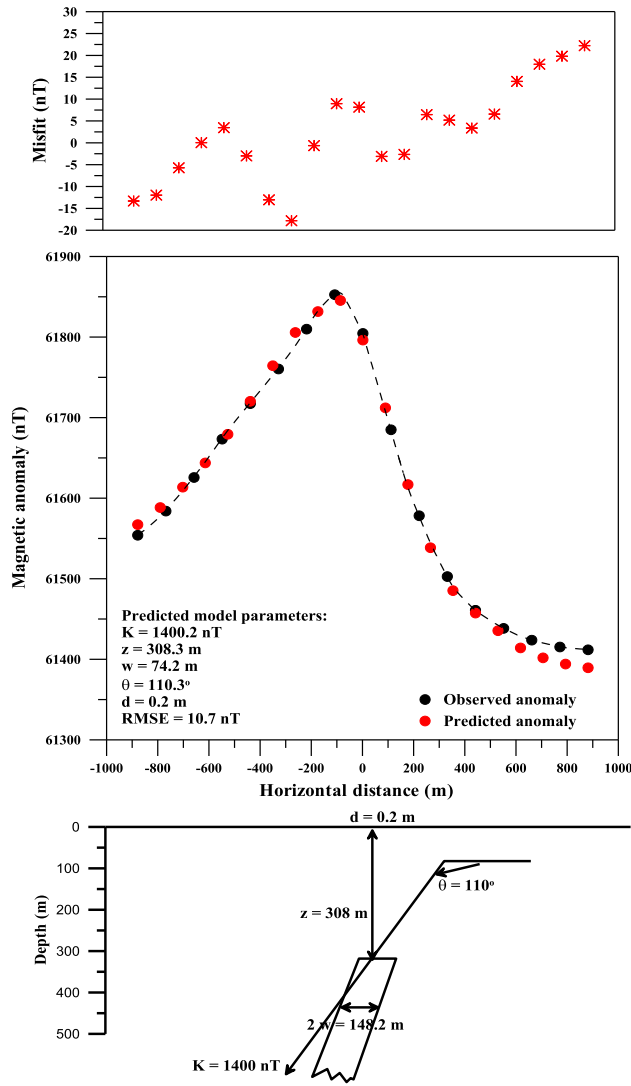


Figure 12. Upper panel: The misfit. Middle panel: Observed (black circles) and predicted anomalies (red circles) for the Pishabo Lake field example, Canada. Lower panel: Geologic section.

Priestley 2008; Cordani *et al.* 2013; Daly *et al.* 2014). Fortes (1978) proposed that ‘the structural tectonic history and shape of this basin are identified with the renaissance of *prior* bedrock structures.’ On the premise of geologic provincial and isotope investigations of a couple of core samples. Neves *et al.* (1984) suggested ‘the presence of a particular yet hidden bedrock mass underneath the central-western part of the basin, caught amongst the craton of Amazon and Borborema orogenic belt’.

Figure 10 demonstrates the observed magnetic anomaly (black circles) due to a structure meddled in the Paleozoic sediments, Parnaiba, Brazil (Abdelrahman *et al.* 2003b). The profile length was 22.4 m and digitised 0.385 m intervals. The digitised anomaly was employed to calculate the dyke parameters employing the particle swarm method

for available residual anomalies produced from applying the second moving average method (figure 11) utilising $s = 0.770, 1.155, 1.540, 1.925, 2.310,$ and 2.695 m. The particle swarm input parameters are the acceleration values equal to 2, inertia value is 0.8, the number of particles is 50, and 400 iterations. Moreover, the range for each dyke parameter is demonstrated in table 3 as ($K = -58.4$ nT, $z = 3.6$ m, $w = 2.3$ m, $\theta = 141.4^\circ$, and $d = 0.6$ m) and also the outcomes. The results of the present inversion method matched well with that given in literary works by other approaches (table 4). Figure 10 shows the predicted anomaly (red circles) compared with the real ones (observed anomaly; black circles). The relationship between the observed and the predicted anomalies exhibited that we found a contrast between them. Silva (1989) demonstrates the distinction because of the weathering of the upper part of the thin sheet.

7.2 Pishabo Lake field example, Canada

The Pishabo Lake is situated in the Cassels Township, District of Nipissing, Ontario, Canada. The north and northwest are characterised by including mafic dykes commonly intruded in the felsic plutonic rocks. These dykes consist of diabase, minor lamprophyre, and plagioclase porphyritic diabase, which are referred to as Matachewan diabase dykes. In addition, this lake is composed of augite, light green and vine, plagioclase, apatite, some biotite, and huge patches of magnetite. Moreover, these dykes are generally 1–3 m wide but reach a maximum of 100 m (Todd 1925; McGrath and Hood 1970; Born 1989; Al-Garni 2017). Naturally, the diabase is huge and fine-to-medium grained with dark grey-green-coloured fresh and weathered surfaces. The minerals consist of actinolite (weakly pleochroic), plagioclase, epidote, quartz, granophyre (plagioclase and quartz intergrowth), per cent chlorite, titanite, and lesser opaque grains.

The magnetic anomaly at Pishabo Lake was described by McGrath and Hood (1970) and Abdelrahman *et al.* (2003b) (figure 12). The profile has 1760 m length and is digitised using a 22-m sampling interval. The second moving average residual anomalies were attained for $s = 44, 66, 88, 110, 132,$ and 154 m (figure 13) using the elucidation processes described above. The particle swarm scheme was applied to those anomalies to estimate the dyke parameters (table 5). The outcomes in

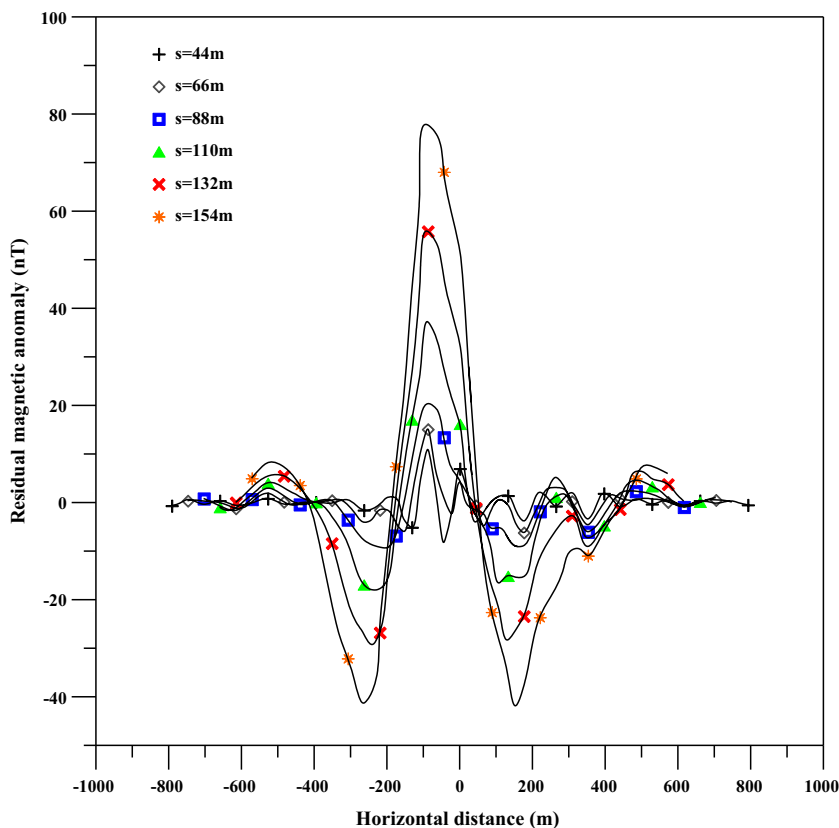


Figure 13. Residual anomaly plots for figure 12.

Table 5. Numerical results for the interpretation of magnetic anomaly of the Pishabo Lake field example, Canada.

Using the PSO-inversion for the second moving average anomalies									
Parameters	Used ranges	$s = 44 \text{ m}$	$s = 66 \text{ m}$	$s = 88 \text{ m}$	$s = 110 \text{ m}$	$s = 132 \text{ m}$	$s = 154 \text{ m}$	ϕ	RMSE (nT)
K (nT)	100–2000	1390.2	1395.1	1400.0	1403.2	1405.7	1406.8	1400.2	10.7
z (m)	50–500	304.1	306.4	308.4	309.1	310.1	311.4	308.3	
w (m)	10–200	71.4	72.5	74.8	74.4	75.8	76.1	74.2	
θ ($^\circ$)	0–180	108.3	110.2	110.6	111.1	111.3	110.1	110.3	
d (m)	–10–10	0.1	0.2	0.1	0.1	0.3	0.2	0.2	

Table 6. Numerical results achieved compared with other results from different approaches for the Pishabo Lake field example, Canada.

Parameters	McGrath and Hood (1970)	Abdelrahman and Essa (2005)	Abdelrahman <i>et al.</i> (2012)	Essa and Elhoussein (2017)	The present method
K (nT)	–	1033	1429	1547.07	1400.2 ± 6.5
z (m)	301.52	311	320	311.46	308.3 ± 2.6
w (m)	–	–	–	44	74.2 ± 1.8
θ ($^\circ$)	106	–	37.3	53.49	110.3 ± 1.1
d (m)	–	–	–	–	0.2 ± 0.1

table 4 are; $K = 1400.2$ nT, $z = 308.3$ m, $w = 74.2$ m, $\theta = 110.3^\circ$, and $d = 0.2$ m.

The results attained from the proposed method are matched alongside those of McGrath and Hood (1970), Tlas and Afahani (2011), Abdelrahman *et al.* (2012), and Essa and Elhussein (2017) (table 6). This table recommends that the approach established here is more beneficial than earlier available methods because it can remove the impeded regional effect and noise in data and execute the optimal buried source parameters with acceptable uncertainties, which are beneficial in exploration geophysics. Figure 12 is explained a judgment amongst the observed (black circles) and predicted (red circles) magnetic anomalies from the proposed method and their misfit.

8. Discussion

In synthetic experiments, we initiate this assessment by utilising the number of particles equals 50 because it depends on the number of unknowns, i.e., the ratio between them is the number of particles equal 8–12 times the unknowns.

Our results of synthetic experiments, which included noise and regional anomalies, explain that the proposed method has proficiency in avoiding the noise and regional anomaly background in the collected magnetic data and gives a respectable view for deducing the subsurface dyke parameters (the magnetic dipole moment, depth, half-width, magnetisation angle, and origin location). Besides, the error in each parameter and the RMSE (misfit) reflect the stability in the obtained results. Furthermore, the attained results for two field cases reflected the accuracy of the present method.

Magnetic anomaly in the Parnaiba basin (Brazil) for a structure meddled in the Palaeozoic sediments (figure 10) has been investigated. The attained results for the impeded dyke structure are matched with available geologic and geophysical information (table 4). For example, the depth deduced by Silva (1989) is 3.5 m and our inversion method is 3.6 m. Also, a magnetic anomaly in the Pishabo Lake area (Canada) to detect a Matachewan diabase dykes (figure 12) was studied. The results achieved were compared alongside those of McGrath and Hood (1970), Tlas and Afahani (2011), Abdelrahman *et al.* (2012), and Essa and Elhussein (2017) (table 6) and found acceptable uncertainties. The patterns of the

estimated magnetic anomaly in the two cases matched well the observed anomalies.

Finally, the motivation for exploiting the particle swarm scheme is to capitalise on its benefits in overwhelming the instability and non-uniqueness of the magnetic anomalies inversion. Also, the method is robust and well-organised in attaining a global solution. Synthetic and field cases declared above explain the power of the proposed method.

9. Conclusions

The use of the particle swarm process along with second moving average anomalies, is likely to be beneficial in geophysical exploration because it proposes various advantages, including (i) it eliminates the influence of deep structure (regional anomaly), (ii) it eradicates the weight of neighbouring structures and noise responses, and (iii) it accurately deduces the inclined dyke model parameters. The proposed method is simple, automatic, and does not need any graphical support. The synthetic examples investigated demonstrated that the suggested scheme is stable in terms of noise and neighbouring bodies effect. It has additionally been successfully applied to two real data sets from Brazil and Canada acquired over mineral deposits and produced positive results. From the validation of the results, this method is robust and firm.

Acknowledgements

We would like to thank Prof. S Dasgupta, Editor-in-Chief, Prof. Munukutla Radhakrishna, Associate Editor, and the reviewer for his keen interest, valuable comments and improvements to this work. Also, the authors would like to express their gratitude to the Institut Francais d’Egypte (IFE) for their complete support in completing this work.

Author statement

Khalid Essa: Conceptualisation, methodology, writing – original draft, review and editing. Eid R Abo-Ezz: Writing – original draft, reviewing, and editing. Yves Géraud: Writing – reviewing, editing, and visualisation. Marc Diraison: Review, editing, and visualisation.

References

- Abdelrahman E M and Essa K S 2005 Magnetic interpretation using a least-squares, depth-shape curves method; *Geophysics* **70** L23–L30.
- Abdelrahman E M, El-Araby T M and Essa K S 2003a Shape and depth solutions from third moving average residual gravity anomalies using the window curves method; *Kuwait J. Sci. Eng.* **30** 95–108.
- Abdelrahman E M, El-Araby T M and Essa K S 2003b A least-squares minimisation approach to depth, index parameter, and amplitude coefficient determination from magnetic anomalies due to thin dykes; *Explor. Geophys.* **34** 241–248.
- Abdelrahman E M, El-Araby H M, El-Araby T M and Essa K S 2003c A least-squares minimisation approach to depth determination from magnetic data; *Pure Appl. Geophys.* **160** 1259–1271.
- Abdelrahman E M, Abo-Ezz E R, Soliman K S, EL-Araby T M and Essa K S 2007 A least-squares window curves method for interpretation of magnetic anomalies caused by dipping dikes; *Pure Appl. Geophys.* **164** 1027–1044.
- Abdelrahman E M, El-Araby T M and Essa K S 2009 Shape and depth determination from second moving average residual self-potential anomalies; *J. Geophys. Eng.* **6** 43–52.
- Abdelrahman E M, Abo-Ezz E R and Essa K S 2012 Parametric inversion of residual magnetic anomalies due to simple geometric bodies; *Explor. Geophys.* **43** 178–189.
- Abdullahi M, Singh U K and Roshan R 2019 Mapping magnetic lineaments and subsurface basement beneath parts of Lower Benue Trough (LBT), Nigeria: Insights from integrating gravity, magnetic and geologic data; *J. Earth Syst. Sci.* **128** 17.
- Acitasa S, Aladag C H and Senoglu B 2019 A new approach for estimating the parameters of Weibull distribution via particle swarm optimisation: An application to the strengths of glass fibre data; *Reliab. Eng. Syst. Saf.* **183** 116–127.
- Adewumi T and Salako K A 2018 Delineation of mineral potential zone using high-resolution aeromagnetic data over part of Nasarawa State, North Central, Nigeria; *Egypt J. Petrol.* **27** 759–767.
- Al-Garni M A 2015 Interpretation of magnetic anomalies due to dipping dikes using neural network inversion; *Arab. J. Geosci.* **8** 8721–8729.
- Al-Garni M A 2017 Inversion of magnetic anomalies due to isolated thin dike-like sources using artificial neural networks; *Arab. J. Geosci.* **10** 337.
- Asfahani J and Tlas M 2007 A robust nonlinear inversion for the interpretation of magnetic anomalies caused by faults, thin dikes and spheres like structure using stochastic algorithms; *Pure Appl. Geophys.* **164** 2023–2042.
- Balkaya Ç and Kaftan I 2021 Inverse modelling via differential search algorithm for interpreting magnetic anomalies caused by 2D dyke-shaped bodies; *J. Earth Syst. Sci.* **130** 135.
- Bhimasankaram V L S, Mohan N I and Seshagiri Rao S V 1978 Interpretation of magnetic anomalies of dikes using Fourier transforms; *Geoexploration* **16** 259–266.
- Biswas A and Acharya T 2016 A very fast simulated annealing method for inversion of magnetic anomaly over semi-infinite vertical rod-type structure; *Model. Earth Syst. Environ.* **2** 1–10.
- Biswas A and Rao K 2021 Interpretation of magnetic anomalies over 2D fault and sheet-type mineralised structures using very fast simulated annealing global optimisation: An understanding of uncertainty and geological implications; *Lithosphere* **2021** 2964057.
- Born P 1989 Precambrian geology Cassels and Riddell Townships; Ontario Geological Survey Report 271.
- Ciuprina G, Ioan D and Munteanu I 2002 Use of intelligent-particle swarm optimisation in electromagnetics; *IEEE Trans. Magn.* **38** 1037–1040.
- Cooper G R J 2012 The semi-automatic interpretation of magnetic dyke anomalies; *Comput. Geosci.* **44** 95–99.
- Cooper G R J 2015 Using the analytic signal amplitude to determine the location and depth of thin dikes from magnetic data; *Geophysics* **80** 1JF-Z39.
- Cordani U G, Pimentel M M, Araujo C E G, Fuck R A *et al.* 2013 The significance of the Transbrasiliano–Kandi tectonic corridor for the amalgamation of West Gondwana; *Braz. J. Geol.* **43** 583–597.
- Daly M C, Andrade V, Barousse C A, Costa R, McDowell K, Piggott N and Poole A J 2014 Brasiliano crustal structure and the tectonic setting of the Parnaíba basin of NE Brazil: Results of a deep seismic reflection profile; *Tectonics* **33** 2102–2120.
- de Castro D L, Bezerra F H, Fuck R A and Vidotti R M 2016 Geophysical evidence of pre-sag rifting and post-rifting fault reactivation in the Parnaíba basin, Brazil; *Solid Earth* **7** 529–548.
- Dondurur D and Pamukçu O A 2003 Interpretation of magnetic anomalies from dipping dike model using inverse solution, power spectrum and Hilbert transform methods; *J. Balkan Geophys. Soc.* **6** 127–139.
- Engelbrecht A P 2007 *Computational intelligence: An introduction*; Wiley & Sons, Ltd.
- Essa K S 2019 A particle swarm optimisation method for interpreting self potential anomalies; *J. Geophys. Eng.* **16** 463–477.
- Essa K S 2021 Evaluation of the parameters of fault-like geologic structure from the gravity anomalies applying the particle swarm; *Environ. Earth Sci.* **80** 489.
- Essa K S and Diab Z E 2022a An automatic inversion approach for magnetic data applying the global bat optimisation algorithm (GBOA): Application to ore deposits and basement rock intrusion; *Geomech. Geophys. Geo-Energ. Geo-Resour.* **8** 185.
- Essa K S and Diab Z E 2022b Magnetic data interpretation for 2D dikes by the metaheuristic bat algorithm: Sustainable development cases; *Sci. Rep.* **12** 14206.
- Essa K S and Elhussein M 2017 A new approach for the interpretation of magnetic data by a 2-D dipping dike; *J. Appl. Geophys.* **136** 431–443.
- Essa K S and Elhussein M 2018 PSO (Particle Swarm Optimisation) for interpretation of magnetic anomalies caused by simple geometrical structures; *Pure Appl. Geophys.* **175** 3539–3553.
- Essa K S and Elhussein M 2019 Magnetic interpretation utilising a new inverse algorithm for assessing the parameters of buried inclined dike-like geological structure; *Acta Geophys.* **67** 533–544.

- Essa K S and Elhussein M 2020 Interpretation of magnetic data through particle swarm optimisation: Mineral exploration cases studies; *Nat. Resour. Res.* **29** 521–537.
- Essa K S and Munsch M 2019 Gravity data interpretation using the particle swarm optimisation method with application to mineral exploration; *J. Earth Syst. Sci.* **128** 123.
- Essa K S, Mehane S and Elhussein M 2021 Magnetic data profiles interpretation for mineralised buried structures identification applying the variance analysis method; *Pure Appl. Geophys.* **178** 973–993.
- Essa K S, Abo-Ezz E R, Géraud Y and Diraison M 2022a A full interpretation applying a metaheuristic particle swarm for gravity data of an active mud diaper, SW Taiwan; *J. Petrol. Sci. Eng.* **215** 110683.
- Essa K S, Munsch M, Yousef M A S and Khalaf E A 2022b Aeromagnetic and radiometric data interpretation to delineate the structural elements and probable Precambrian mineralisation zones: A case study, Egypt; *Min. Metall. Explor.* **39** 2461–2475.
- Fortes F P 1978 Geologia Estrutural e Tectonica da Bacia Sedimentar do Meio Norte do Brasil; *Annual 30th Congress Brasil Geologia* **1** 321–336.
- Gay S P 1963 Standard curves for interpretation of magnetic anomalies over long tabular bodies; *Geophysics* **28** 161–200.
- Gionfra N, Sandou G, Siguerdidjane H, Faille D and Loevenbruck P 2019 Wind farm distributed PSO-based control for constrained power generation maximisation; *Renew. Energy* **133** 103–117.
- Godio A and Santilano A 2018 On the optimisation of electromagnetic geophysical data: Application of the PSO algorithm; *J. Appl. Geophys.* **148** 163–174.
- Gokula A P and Sastry R G 2022 Total magnetic-field intensity anomaly due to a vertical pyramid model of flat top and bottom with constant magnetisation; *J. Earth Syst. Sci.* **131** 8.
- Griffin W R 1949 Residual gravity in theory and practice; *Geophysics* **14** 39–58.
- Johnson W W 1969 A least squares method of interpreting magnetic anomalies caused by two dimensional structures; *Geophysics* **34** 65–74.
- Kara İ, Tarhan Bal O, Tekkeli A B and Karcioğlu G 2017 A different method for interpretation of magnetic anomalies due to 2-D dipping dikes; *Acta Geophys.* **65** 237.
- Keating P B and Pilkington M 1990 An automated method for the interpretation of magnetic vertical-gradient anomalies; *Geophysics* **55** 336–343.
- Kennedy J and Eberhart R 1995 Particle Swarm Optimisation; *Proc. IEEE Int. Conf. Neural Netw.* **4** 1942–1948.
- Kennedy J, Eberhart R and Shi Y H 2001 *Swarm intelligence*; Morgan Kaufmann Publishers.
- Koulomzine T, Lamontagne Y and Nadeau A 1970 New methods for the direct interpretation of magnetic anomalies caused by inclined dikes of infinite length; *Geophysics* **35** 812–830.
- Lehmann J, Master S, Rankin W, Milani L, Kinnaird J A, Naydenova K V, Saalman K and Kumar M 2015 Regional aeromagnetic and stratigraphic correlations of the Kalahari Copperbelt in Namibia and Botswana; *Ore Geol. Rev.* **71** 169–190.
- Li R, Zhang H, Yu N, Li R and Zhuang Q 2019 A fast approximation for 1-D inversion of transient electromagnetic data by using a back propagation neural network and improved particle swarm optimisation; *Nonlinear Process. Geophys.* **26** 445–456.
- Mandal A, Chandroth A, Basantaray A K *et al.* 2020 Delineation of shallow structures in Madawara igneous complex, Bundelkhand Craton, India using gravity–magnetic data: Implication to tectonic evolution and mineralisation; *J. Earth Syst. Sci.* **129** 90.
- McGrath P H and Hood P J 1970 The dipping dike case: A computer curve-matching method of magnetic interpretation; *Geophysics* **35** 831–848.
- McKenzie D P and Priestley K 2008 The influence of lithospheric thickness variation on continental evolution; *Lithos* **102** 1–11.
- Mehane S A 2022 Simultaneous Joint Inversion of Gravity and Self-Potential Data Measured along Profile: Theory, Numerical Examples, and a Case Study from Mineral Exploration with Cross Validation from Electromagnetic Data; *IEEE Trans. Geosci. Remote Sens.* **60** 1–20.
- Mehane S, Essa K S and Diab Z E 2021 Magnetic data interpretation using a new R-parameter imaging method with application to mineral exploration; *Nat. Resour. Res.* **30** 77–95.
- Neves B B, Fuck R A, Cordani U G, Thomaz A *et al.* 1984 Influence of basement structures on the evolution of the major sedimentary basins of Brazil: A case of tectonic heritage; *J. Geodyn.* **1** 495–510.
- Qianwei D, Hao Z and Bin Z 2021 An improved particle swarm optimisation based on total variation regularisation and projection constraint with applications in ground-penetrating radar inversion: A model simulation study; *Remote Sens.* **13** 2514.
- Ramesh B N, Nagaraju E, Parashuramulu V and Venkateshwarlu M 2020 Preliminary anisotropy of magnetic susceptibility studies on 2367 Ma Bangalore–Karimnagar giant dyke swarm, southern India: Implications for magma flow; *Phys. Earth Planetet. Int.* **306** 106540.
- Rao B S R, Prakasa Rao T K S, Gopala Rao D and Kesavamani M 1972 Derivatives and dike anomaly interpretation; *Pure Appl. Geophys.* **99** 120–129.
- Roy A, Dubey C P and Prasad M 2021 Gravity inversion of basement relief using Particle Swarm Optimisation by automated parameter selection of Fourier coefficients; *Comput. Geosci.* **156** 104875.
- Sengupta S and Das S K 1975 Interpretation of magnetic anomalies of dikes by Fourier transforms; *Pure Appl. Geophys.* **113** 625–633.
- Sharma P V 1987 Magnetic method applied to mineral exploration; *Ore Geol. Rev.* **2** 323–357.
- Silva J B C 1989 Transformation of nonlinear problems into linear ones applied to the magnetic field of a two-dimensional prism; *Geophysics* **54** 114–121.
- Singh A and Biswas A 2016 Application of global particle swarm optimisation for inversion of residual gravity anomalies over geological bodies with idealised geometries; *Nat. Resour. Res.* **25** 297–314.
- Tlas M and Asfahani J 2011 Fair function minimisation for interpretation of magnetic anomalies due to thin dikes, spheres and faults; *J. Appl. Geophys.* **75** 237–243.
- Tlas M and Asfahani J 2015 The simplex algorithm for best-estimate of magnetic parameters related to simple geometric-shaped structures; *Math. Geosci.* **47** 301–316.

- Todd E W 1925 The Matabitchuan area Ont. Dept. curves; *Geophysics* **31** 135–148.
- Werner S 1953 Interpretation of magnetic anomalies of sheet-like bodies; Sveriges Geologiska Undersökning, Series C, Årsbok 43, No. 6.
- Won I J 1981 Application of Gauss's method to magnetic anomalies of dipping dikes; *Geophysics* **46** 211–215.
- Yang Y, Wen J and Chen X 2015 Improvements on particle swarm optimisation algorithm for velocity calibration in microseismic monitoring; *Earthq. Sci.* **28** 263–273.
- Yin Z, Jin Y, Shen J S and Hicher P 2018 Optimisation techniques for identifying soil parameters in geotechnical engineering: Comparative study and enhancement; *Int. J. Numer. Anal. Methods* **42** 70–94.

Corresponding editor: SOMNATH DASGUPTA